

Photoproduction of dileptons and photons in p - p collisions at the Large Hadron Collider energies

Zhi-Lei Ma and Jia-Qing Zhu

*Department of Physics, Yunnan University, Kunming 650091, China
and Key Laboratory of Astroparticle Physics of Yunnan Province, Yunnan University,
Kunming 650091, China*

 (Received 8 September 2017; revised manuscript received 22 December 2017; published 26 March 2018)

The production of large p_T dileptons and photons originating from photoproduction processes in p - p collisions at Large Hadron Collider energies is calculated. The comparisons between the exact treatment results and the ones of the equivalent photon approximation approach are expressed as the Q^2 (the virtuality of photon) and p_T distributions. The method developed by Martin and Ryskin is used for avoiding double counting when the coherent and incoherent contributions are considered simultaneously. The numerical results indicate that the equivalent photon approximation is only effective in small Q^2 region and can be used for coherent photoproduction processes with proper choice of Q_{\max}^2 (the choices $Q_{\max}^2 \sim \hat{s}$ or ∞ will cause obvious errors), but cannot be used for incoherent photoproduction processes. The exact treatment is needed to deal accurately with the photoproduction of large p_T dileptons and photons.

DOI: [10.1103/PhysRevD.97.054030](https://doi.org/10.1103/PhysRevD.97.054030)

I. INTRODUCTION

Since its conveniences and simplicity, the equivalent photon approximation (EPA), which can be traced to early work by Fermi, Weizsäcker and Williams (1934), and Landau and Lifshitz (1934), has been widely used for the approximate calculation of the various processes in relativistic heavy ion collisions [1–7]. By treating the moving electromagnetic fields of charged particles as a flux of real photons, many topics are studied such as photoproduction mechanism, particle and particle pairs production, meson production in electron-nucleon collisions, two-photon particle production mechanism, the determining of the nuclear parton distributions, and small x physics [8–18]. The accuracy of the EPA is denoted by a dynamical cut-off Λ_γ^2 of the photon virtuality Q^2 . At $Q^2 < \Lambda_\gamma^2$, photo-absorption cross sections differ slightly from their values on the mass shell and quickly decrease at $Q^2 > \Lambda_\gamma^2$. Thus, the EPA approach is a reasonable approximation comparing with the exact treatment which returns to the EPA approach when $Q^2 \rightarrow 0$, and is used precisely for the description of the cross sections only at the kinematics domain $Q^2 < \Lambda_\gamma^2$ [18–21]. However, the applicability range of EPA and of its accuracy are not always considered in most works where Q_{\max}^2 is usually set to be $\hat{s}/4$ (\hat{s} is the squared center-of-mass (CM) frame energy of the photo-absorption processes) or even infinity, which will cause a large fictitious contribution from the $Q^2 > \Lambda_\gamma^2$ domain [17]. On the other hand, the EPA approach can not be used for the study of the incoherent photon emission processes since the parton-quark model is used which requires Q^2 should be larger than Λ_{QCD} , and

some statements in the previous studies [9–14] are actually inaccurate.

Hadronic processes for producing large transverse momentum (p_T) dileptons and photons are very important in the research of relativistic p - p collisions. Since photons and dileptons do not participate in the strong interactions directly, the photon or dilepton production can test the predictions of perturbative quantum chromodynamics (pQCD) calculations, and has long been proposed as ideal probes of the strong interacting matter (quark-gluon plasma, QGP) properties without the interference of final-state interactions. In the present work, we extend the photoproduction mechanism which plays a fundamental role in the ep deep inelastic scattering at the Hadron Electron Ring Accelerators [22–25] to the production of large p_T photons and dileptons in p - p collisions at Large Hadron Collider (LHC) energies, which has been investigated in most literatures in the EPA approach. There are several motivations. Although the hard scattering of initial partons (the annihilation and Compton scattering of partons) is a dominant source of large p_T dileptons and photons in central collisions, the photoproduction processes also playing an interesting role at LHC energies in which its corrections to the production of dileptons and photons are non-negligible (especially at the large p_T domain) [11,12]; The photoproduction processes give the main contribution to the lepton pair production cross section in the peripheral collisions (especially for the ultraperipheral collisions); The EPA is used as an important method in hadronic processes, its validity is not obvious. Therefore, it is meaningful to study the accuracy of EPA in

photoproduction processes and give the accurate corrections to the production of dileptons and photons.

We present the comparisons between EPA approach and exact treatment in which the photon radiated from proton or its constituents is off mass shell and no longer transversely polarized, and the minimum of p_T is chosen as $p_{T\min} = 1$ GeV for satisfying the requirement of pQCD [11,26]. There are two types of photoproduction processes: direct photoproduction processes (dir.pho) and resolved photoproduction processes (res.pho) [11,12]. In the first type, the high-energy photon which are emitted from proton or the charged parton of the incident proton interacts with the parton of another incident proton by quark-photon Compton scattering. In the second type, the high-energy photon, which can be regard as an extend object consisting of quarks and gluons, fluctuates into a quark-antiquark pair for a short time which then interacts with the parton of another incident proton by quark-gluon Compton scattering and quark-antiquark annihilation. Besides, it is necessary to distinguish two kinds of photons emission mechanisms [27,28]: coherent emission in which virtual photons are emitted coherently by the whole proton and the proton remains intact after the photon radiated; incoherent emission in which virtual photons are emitted incoherently by the individual constituents (quarks) of proton and the proton will dissociate or excite after the photon emitted. In most instances, these two kinds of photon emission processes are performed simultaneously, hence the square of the form factor $F_1^2(Q^2)$ is used as coherent probability or weighting factor (WF) for recognizing the coherent part from the whole interaction. In Ref. [29], Martin and Ryskin have been used this method to avoid the double counting in the calculation.

The paper is organized as follows. Section II presents the formalism of exact treatment for the photoproduction of large p_T dileptons and photons in p-p collisions. Based on the method of Martin and Ryskin, the coherent and incoherent contributions are considered simultaneously. The EPA approach is also introduced by taking $Q^2 \rightarrow 0$. In Sec. III, the numerical results with the distributions of Q^2 and p_T at LHC energies are illustrated. Finally, the summary and conclusions are given in Sec. IV.

II. PHOTOPRODUCTION OF LARGE p_T DILEPTONS AND PHOTONS

Since photons and dileptons are the ideal probes in the research of QGP, its production processes have received many studies in EPA approach. Although the EPA has been widely used as a convenient method for the approximate calculation of Feynman diagrams for the collision of fast charged particles [17], it's applicability range is often ignored. Thus, the more precise calculations for the cross sections are needed. We present the exact treatment, which expand the proton or quark tensor (multiplied by Q^{-2}) by using the transverse and longitudinal polarization operators, for the photoproduction of large p_T dileptons

and photons in p-p collisions. The formalism is analogous with Refs. [28,30] where the exact treatment for the photoproduction of heavy quarkonia are studied.

A. The Q^2 distribution of large p_T dilepton production

The large p_T dileptons produced by direct photoproduction processes can be divided into the coherent direct photoproduction processes (coh.dir) and incoherent direct photoproduction processes (incoh.dir). For the case of coh.dir (Fig. 1), the invariant cross section of large p_T dileptons with Q^2 distribution is given by

$$\begin{aligned} & \frac{d\sigma^{\text{coh.dir}}(p + p \rightarrow p + l^+l^- + X)}{dM^2 dQ^2} \\ &= 2 \sum_b \int dy dx_b d\hat{t} f_{b/p}(x_b, \mu_b^2) \\ & \times \frac{d\sigma(p + b \rightarrow p + l^+l^- + b)}{dM^2 dQ^2 dy d\hat{t}}, \end{aligned} \quad (1)$$

where $x_b = p_b/P_B$ is the parton's momentum fraction, $f_{b/p}(x_b, \mu_b^2)$ is the parton distribution function of the proton B [31], and the factorized scale is chosen as $\mu_b = \sqrt{4p_T^2}$ [11]. The cross section of the subprocess $p + b \rightarrow p + l^+l^- + b$ can be written as [28,32]

$$\begin{aligned} & \frac{d\sigma(p + b \rightarrow p + l^+l^- + b)}{dM^2 dQ^2 dy} \\ &= \frac{\alpha}{3\pi M^2} \sqrt{1 - \frac{4m_l^2}{M^2}} \left(1 + \frac{2m_l^2}{M^2}\right) \frac{d\sigma(p + b \rightarrow p + \gamma^* + b)}{dQ^2 dy} \\ &= \frac{\alpha^2}{6\pi^2 M^2} \sqrt{1 - \frac{4m_l^2}{M^2}} \left(1 + \frac{2m_l^2}{M^2}\right) T_{\mu\nu} \frac{y p_{\text{coh}}^{\mu\nu}}{Q^2} \\ & \times \frac{d\text{PS}_2(q + p_b; p_c, p_d)}{2y x_b s_{NN}}, \end{aligned} \quad (2)$$

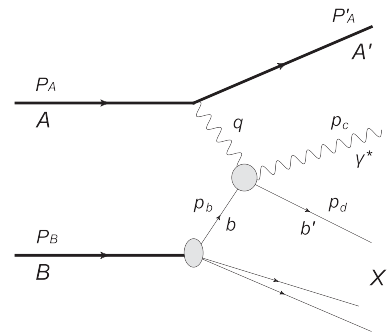


FIG. 1. The coherent direct photoproduction processes in which the virtual photon emitted from the whole incident proton A interacts with parton b of another incident proton B via photon-quark Compton scattering, and A remains intact after the photon emitted. A' is the scattered proton A, b' is the scattered parton b, and X is the sum of residue of B after photon emitted.

where $Q^2 = -q^2$, $y = (q \cdot p_b)/(P_A \cdot p_b)$, M is the invariant mass of dileptons, m_l is lepton mass, $T_{\mu\nu}$ is the amplitude of reaction $\gamma^* + b \rightarrow \gamma^* + b$, s_{NN} is the CM frame energy square of the p-p collision, $dPS_2(q + p_b; p_c, p_d)$ is the Lorentz-invariant phase-space measure [30], the electromagnetic coupling constant is chosen as $\alpha = 1/137$, and

$$\rho_{\text{coh}}^{\mu\nu} = \left(-g^{\mu\nu} + \frac{q^\mu q^\nu}{q^2} \right) H_2(Q^2) - \frac{(2P_A - q)^\mu (2P_A - q)^\nu}{q^2} H_1(Q^2), \quad (3)$$

is the proton tensor (multiplied by Q^{-2}), $H_1(Q^2)$ and $H_2(Q^2)$ are the elastic form factors of proton.

Similarly, the invariant cross section of large p_T dileptons produced by incoh.dir (Fig. 2) with Q^2 distribution has the form

$$\frac{d\sigma^{\text{incoh.dir}}(p + p \rightarrow X_A + l^+ l^- + X)}{dM^2 dQ^2} = 2 \sum_{a,b} \int dy dx_a dx_b d\hat{t} f_{a/p}(x_a, \mu_a^2) f_{b/p}(x_b, \mu_b^2) \frac{d\sigma(a + b \rightarrow a + l^+ l^- + b)}{dM^2 dQ^2 dy d\hat{t}}, \quad (4)$$

where $x_a = p_a/P_A$ is parton's momentum fraction, $f_{a/p}(x_a, \mu_a^2)$ is the parton distribution function of the proton A, $\mu_a = \sqrt{4p_T^2}$. And the cross section of the partonic processes $a + b \rightarrow a + l^+ l^- + b$ reads

$$\begin{aligned} \frac{d\sigma(a + b \rightarrow a + l^+ l^- + b)}{dM^2 dQ^2 dy} &= \frac{\alpha}{3\pi M^2} \sqrt{1 - \frac{4m_l^2}{M^2}} \left(1 + \frac{2m_l^2}{M^2} \right) \frac{d\sigma(a + b \rightarrow a + \gamma^* + b)}{dQ^2 dy} \\ &= \frac{\alpha^2}{6\pi^2 M^2} \sqrt{1 - \frac{4m_l^2}{M^2}} \left(1 + \frac{2m_l^2}{M^2} \right) T_{\mu\nu} \frac{e_a^2 y \rho_{\text{incoh}}^{\mu\nu}}{Q^2} \frac{dPS_2(q + p_b; p_c, p_d)}{2y x_a x_b s_{NN}}, \end{aligned} \quad (5)$$

where e_a is the charge of massless quark a, $y = (q \cdot p_b)/(p_a \cdot p_b)$ for the case of incoh.pho, and the massless quark tensor (multiplied by Q^{-2}) is

$$\rho_{\text{incoh}}^{\mu\nu} = \left(-g^{\mu\nu} + \frac{q^\mu q^\nu}{q^2} \right) L_2(Q^2) - \frac{(2p_a - q)^\mu (2p_a - q)^\nu}{q^2} L_1(Q^2). \quad (6)$$

In Martin-Ryskin method [29], the coherent probability (WF) is given by the square of the form factor $F_1^2(Q^2)$. Therefore,

$$H_1(Q^2) = H_2(Q^2) = F_1^2(Q^2), \quad (7)$$

where $F_1(Q^2)$ can be parametrized by the dipole form: $F_1(Q^2) = (1 + Q^2/0.71 \text{ GeV}^2)^{-2}$.

For the incoherent contribution, the ‘‘remaining’’ probability has to be considered for avoiding double counting, and $L_1(Q^2)$, $L_2(Q^2)$ in Eq. (6) have the forms of

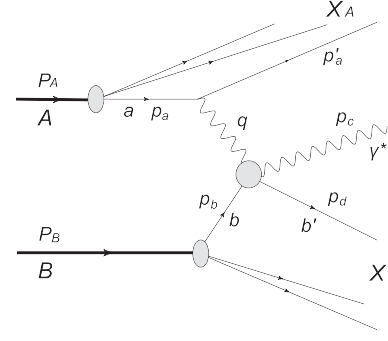


FIG. 2. The incoherent direct photoproduction processes in which virtual photon emitted from the parton a of incident proton A interacts with parton b from proton B via the photon-quark interaction, and A is allowed to break up after photon emitted. a denotes the parton of A, X_A is the residue of A after photon emitted.

$$L_1(Q^2) = L_2(Q^2) = 1 - F_1^2(Q^2). \quad (8)$$

By using the linear combinations [17]

$$\begin{aligned} Q^\mu &= \sqrt{\frac{-q^2}{(q \cdot p_b)^2 - q^2 p_b^2}} \left(p_b - q \frac{q \cdot p_b}{q^2} \right)^\mu, \\ R^{\mu\nu} &= -g^{\mu\nu} + \frac{1}{q \cdot p_b} (q^\mu p_b^\nu + q^\nu p_b^\mu) - \frac{q^2}{(q \cdot p_b)^2} p_b^\mu p_b^\nu, \end{aligned} \quad (9)$$

$\rho^{\mu\nu}$ can be written in the form

$$\rho^{\mu\nu} = \rho^{00} Q^\mu Q^\nu + \rho^{++} R^{\mu\nu}. \quad (10)$$

Apparently, $R^{\mu\nu}$ and $Q^\mu Q^\nu$ are equivalent to transverse and longitudinal polarization [30]: $R^{\mu\nu} = \varepsilon_T^{\mu\nu}$, $Q^\mu Q^\nu = -\varepsilon_L^{\mu\nu}$. Thus, the cross section of subprocesses $p + b \rightarrow p + \gamma^* + b$ can be expressed as [28]

$$\begin{aligned} & \frac{d^3\sigma(p+b \rightarrow p+\gamma^*+b)}{dydQ^2d\hat{t}} \\ &= \frac{\alpha}{2\pi} \left[\frac{y\rho_{\text{coh}}^{++}}{Q^2} \frac{d\sigma_T(\gamma^*+b \rightarrow \gamma^*+b)}{d\hat{t}} \right. \\ & \quad \left. + \frac{y\rho_{\text{coh}}^{00}}{Q^2} \frac{d\sigma_L(\gamma^*+b \rightarrow \gamma^*+b)}{d\hat{t}} \right], \end{aligned} \quad (11)$$

where

$$\begin{aligned} \rho_{\text{coh}}^{++} &= F_1^2(Q^2) \left[\frac{1+(1-y)^2}{y^2} - \frac{2m_p^2}{Q^2} \right] \\ \rho_{\text{coh}}^{00} &= F_1^2(Q^2) \frac{4(1-y)}{y^2}, \end{aligned} \quad (12)$$

$d\sigma_T/d\hat{t}$ and $d\sigma_L/d\hat{t}$ represent the transverse and longitudinal cross sections of subprocesses $\gamma^*+b \rightarrow \gamma^*+b$ respectively,

$$\begin{aligned} & \frac{d\hat{\sigma}_T(\gamma^*+b \rightarrow \gamma^*+b)}{d\hat{t}} \\ &= \frac{4\pi\alpha^2 e_b^4 z^2}{Q^4} \left[-\frac{\hat{t}}{\hat{s}} - \frac{\hat{s}}{\hat{t}} - M^2 Q^2 \left(\frac{1}{\hat{s}^2} + \frac{1}{\hat{t}^2} \right) \right. \\ & \quad \left. + 2(Q^2 - M^2) \frac{\hat{u}}{\hat{s}\hat{t}} \right] + \frac{8\pi\alpha^2 e_b^4 z^2 Q^2 \hat{u}(\hat{t} - M^2)^2}{Q^4 \hat{t}^2(\hat{s} + Q^2)^2}, \end{aligned} \quad (13)$$

and

$$\frac{d\hat{\sigma}_L(\gamma^*+b \rightarrow \gamma^*+b)}{d\hat{t}} = \frac{8\pi\alpha^2 e_b^4 z^2 Q^2 \hat{u}(\hat{t} - M^2)^2}{Q^4 \hat{t}^2(\hat{s} + Q^2)^2}, \quad (14)$$

where $z = Q^2/(\hat{s} + Q^2)$, e_b is the charge of massless quark b . The Mandelstam variables for subprocesses $\gamma^*+b \rightarrow \gamma^*+b$ are defined as

$$\begin{aligned} \hat{s} &= (q+p_b)^2 = \frac{M^2}{z_q} + \frac{p_T^2}{z_q(1-z_q)}, \\ \hat{t} &= (q-p_c)^2 = (z_q-1)yx_b s_{NN}, \\ \hat{u} &= (p_b-p_c)^2 = M^2 - z_q y x_b s_{NN}, \end{aligned} \quad (15)$$

where $z_q = (p_c \cdot P_B)/(q \cdot P_B)$ is the inelasticity variable, p_T is the transverse momentum in the γ^*-b CM frame.

In the same way, we can write the cross section of the incoherent subprocesses $a+b \rightarrow a+\gamma^*+b$ as

$$\begin{aligned} & \frac{d^3\sigma(a+b \rightarrow a+\gamma^*+b)}{dydQ^2d\hat{t}} \\ &= \frac{\alpha}{2\pi} e_a^2 \left[\frac{y\rho_{\text{incoh}}^{++}}{Q^2} \frac{d\sigma_T(\gamma^*+b \rightarrow \gamma^*+b)}{d\hat{t}} \right. \\ & \quad \left. + \frac{y\rho_{\text{incoh}}^{00}}{Q^2} \frac{d\sigma_L(\gamma^*+b \rightarrow \gamma^*+b)}{d\hat{t}} \right], \end{aligned} \quad (16)$$

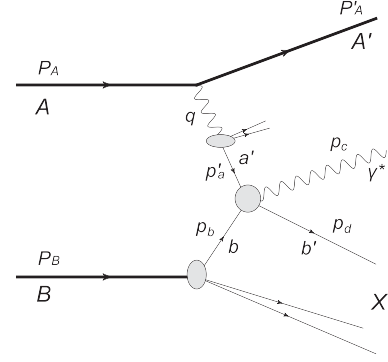


FIG. 3. The coherent resolved photoproduction processes in which the incident proton A emits a high energy virtual photon, then the parton a' of the resolved photon interacts with the parton b of another incident proton B via the interactions of quark-antiquark annihilation and quark-gluon Compton scattering, and the proton A remains intact after photon emitted.

where

$$\begin{aligned} \rho_{\text{incoh}}^{++} &= (1 - F_1^2(Q^2)) \frac{1+(1-y)^2}{y^2} \\ \rho_{\text{incoh}}^{00} &= (1 - F_1^2(Q^2)) \frac{4(1-y)}{y^2}, \end{aligned} \quad (17)$$

here we have $\hat{s} = M^2/z_q + p_T^2/(z_q - z_q^2)$, $\hat{t} = (z_q - 1)yx_a x_b s_{NN}$ and $\hat{u} = M^2 - z_q y x_a x_b s_{NN}$.

The resolved photoproduction processes are very important in the research of relativistic heavy ion collisions. The resolved photoproduction processes can also be divided into two categories: coherent resolved photoproduction processes (coh.res) and incoherent resolved photoproduction processes (incoh.res). In the case of coh.res (Fig. 3), the invariant cross section of large p_T dileptons with Q^2 distribution is

$$\begin{aligned} & \frac{d\sigma^{\text{coh.res}}(p+p \rightarrow p+l^+l^-+X)}{dM^2 dQ^2} \\ &= 2 \sum_b \sum_{a'} \int dy dx_b dz_{a'} d\hat{t} f_{b/p}(x_b, \mu_b^2) f_{\gamma}(z_{a'}, \mu_\gamma^2) \\ & \quad \times \frac{\alpha}{2\pi} \frac{y\rho_{\text{coh}}^{++}}{Q^2} \frac{d\sigma(a'+b \rightarrow \gamma^*+b)}{dM^2 d\hat{t}}, \end{aligned} \quad (18)$$

where $z_{a'}$ denotes the parton's momentum fraction of the resolved photon which are emitted from the proton A, $f_\gamma(z_{a'}, \mu_\gamma^2)$ is the parton distribution function of the resolved photon [33], $\mu_\gamma = \sqrt{4p_T^2}$. The cross sections of subprocesses $a'+b \rightarrow \gamma^*+b$ are given by

$$\begin{aligned} \frac{d\hat{\sigma}}{d\hat{t}}(q\bar{q} \rightarrow \gamma^*\gamma) &= \frac{2\pi\alpha^2 e_q^4}{3} \frac{\hat{t}_\gamma}{\hat{s}_\gamma^2} \left(\frac{\hat{t}_\gamma}{\hat{u}_\gamma} + \frac{\hat{u}_\gamma}{\hat{t}_\gamma} + \frac{2M^2 \hat{s}_\gamma}{\hat{u}_\gamma \hat{t}_\gamma} \right) \\ \frac{d\hat{\sigma}}{d\hat{t}}(q\bar{q} \rightarrow \gamma^*g) &= \frac{8\pi\alpha\alpha_s e_q^2}{9} \frac{\hat{t}_\gamma}{\hat{s}_\gamma^2} \left(\frac{\hat{t}_\gamma}{\hat{u}_\gamma} + \frac{\hat{u}_\gamma}{\hat{t}_\gamma} + \frac{2M^2 \hat{s}_\gamma}{\hat{u}_\gamma \hat{t}_\gamma} \right) \\ \frac{d\hat{\sigma}}{d\hat{t}}(qg \rightarrow \gamma^*q) &= \frac{1\pi\alpha\alpha_s e_q^2}{3} \frac{\hat{t}_\gamma}{\hat{s}_\gamma^2} \left(-\frac{\hat{t}_\gamma}{\hat{s}_\gamma} - \frac{\hat{s}_\gamma}{\hat{t}_\gamma} - \frac{2M^2 \hat{u}_\gamma}{\hat{s}_\gamma \hat{t}_\gamma} \right). \end{aligned} \quad (19)$$

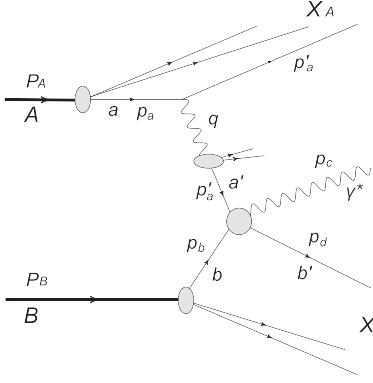


FIG. 4. The incoherent resolved photoproduction processes in which the parton a' of the resolved photon radiated by parton a of proton A interacts with the parton b from proton B via the quark-antiquark annihilation and quark-gluon Compton scattering, and A is allowed to break up after photon emitted.

where $\hat{s}_\gamma = M^2/z'_q + p_T^2/(z'_q - z_q'^2)$, $\hat{t}_\gamma = (z'_q - 1)\hat{s}_\gamma$, and $\hat{u}_\gamma = M^2 - z'_q\hat{s}_\gamma$ are the Mandelstam variables for the subprocesses of res.pho, $z'_q = (p_c \cdot p_b)/(p_{a'} \cdot p_b)$ is the inelasticity variable. The strong coupling constant is taken as the one-loop form [34]

$$\alpha_s = \frac{12\pi}{(33 - 2n_f) \ln(\mu^2/\Lambda^2)}, \quad (20)$$

with $n_f = 3$ and $\Lambda = 0.2$ GeV.

The invariant cross section for large p_T dileptons produced by incoh.res (Fig. 4) with Q^2 distribution can be presented as

$$\begin{aligned} & \frac{d\sigma^{\text{incoh.res}}(p + p \rightarrow X_A + l^+l^- + X)}{dM^2 dQ^2} \\ &= 2 \sum_{a,b} \sum_{a'} \int dy dx_a dx_b dz_{a'} d\hat{t} f_{a/p}(x_a, \mu_a^2) f_{b/p}(x_b, \mu_b^2) \\ & \times f_\gamma(z_{a'}, \mu_\gamma^2) e_a^2 \frac{\alpha}{2\pi} \frac{y \rho_{\text{incoh}}^{++}}{Q^2} \frac{d\sigma(a' + b \rightarrow \gamma^* + b)}{dM^2 d\hat{t}}, \end{aligned} \quad (21)$$

the cross sections of subprocesses $a' + b \rightarrow \gamma^* + b$ are discussed in Eq. (19).

B. The p_T distribution of large p_T dileptons production

It is straightforward to obtain the distribution of p_T by accordingly reordering and redefining the integration variables in Eq. (1). For convenience, the Mandelstam variables in Eq. (15) can be written in the form

$$\begin{aligned} \hat{s} &= 2 \cosh y_r M_T \sqrt{\cosh^2 y_r M_T^2 - M^2} \\ & \quad + 2 \cosh^2 y_r M_T^2 - M^2, \\ \hat{t} &= M^2 - Q^2 - \sqrt{\hat{s}} M_T e^{-y_r} + \frac{Q^2}{\sqrt{\hat{s}}} M_T e^{y_r}, \\ \hat{u} &= M^2 - \sqrt{\hat{s}} M_T e^{y_r} - \frac{Q^2}{\sqrt{\hat{s}}} M_T e^{y_r}, \end{aligned} \quad (22)$$

where $y_r = \ln(\cot \theta_c/2)$ is the rapidity, θ_c is the CM frame scattering angle, $M_T = \sqrt{p_T^2 + M^2}$ is the dileptons transverse mass. By using the Jacobian determinant, the variables x_b and \hat{t} can be transformed into

$$d\hat{t} dx_b = \left| \frac{D(x_b, \hat{t})}{D(p_T, y_r)} \right| dy_r dp_T^2, \quad (23)$$

where the Jacobian determinant is

$$\begin{aligned} & \left| \frac{D(x_b, \hat{t})}{D(p_T, y_r)} \right| \\ &= \frac{\cosh y_r}{y s_{NN} \sqrt{\cosh^2 y_r M_T^2 - M^2}} \left[M_T \left(2 \cosh y_r \right. \right. \\ & \quad \left. \left. + \frac{2 \cosh^2 y_r M_T^2 - M^2}{M_T \sqrt{\cosh^2 y_r M_T^2 - M^2}} \right) \left(M_T \sqrt{\hat{s}} - M^2 e^{y_r} \right) \right. \\ & \quad \times \left(e^{-2y_r} + \frac{Q^2}{\hat{s}} \right) + \sinh y_r \left(\hat{s} e^{-y_r} + \frac{Q^2 M^2 e^{y_r}}{\hat{s}} \right) \\ & \quad \left. \times \left(2M_T + \frac{2 \cosh^2 y_r M_T^2 - M^2}{\cosh y_r \sqrt{\cosh^2 y_r M_T^2 - M^2}} \right) \right]. \end{aligned} \quad (24)$$

Thus, the invariant cross section of large p_T dileptons produced by coh.dir with p_T distribution can be expressed as

$$\begin{aligned} & \frac{d\sigma_{y_{rc}}^{\text{coh.dir}}(p + p \rightarrow p + l^+l^- + X)}{dM^2 dp_T^2 dy_r} \\ &= 2 \sum_b \int dQ^2 dy f_{b/p}(x_b, \mu_b^2) \frac{\hat{s}}{y s_{NN} p_T} \left(\sqrt{\hat{s}} + \frac{Q^2}{\sqrt{\hat{s}}} \right) \\ & \quad \times \frac{d\sigma(p + b \rightarrow p + l^+l^- + b)}{dM^2 dQ^2 dy d\hat{t}}, \end{aligned} \quad (25)$$

where y_{rc} represents that the cross section is calculated at $y_r = 0$, the cross section $d\sigma(p + b \rightarrow p + l^+l^- + b)/(dM^2 dQ^2 dy d\hat{t})$ is discussed in Eqs. (2) and (11).

In the case of incoh.dir, the invariant cross section for large p_T dileptons with p_T distribution is given by

$$\begin{aligned}
& \frac{d\sigma_{yrc}^{\text{incoh.dir}}(p+p \rightarrow X_A + l^+l^- + X)}{dM^2 dp_T^2 dy_r} \\
&= 2 \sum_{a,b} \int dQ^2 dy dx_a f_{a/p}(x_a, \mu_a^2) f_{b/p}(x_b, \mu_b^2) \\
& \quad \times \frac{\hat{s}}{y x_a s_{NN} p_T} \left(\sqrt{\hat{s}} + \frac{Q^2}{\sqrt{\hat{s}}} \right) \frac{d\sigma(a+b \rightarrow a+l^+l^-+b)}{dM^2 dQ^2 dy d\hat{t}}, \quad (26)
\end{aligned}$$

the Mandelstam variables are the same as Eq. (22), the cross section $d\sigma(a+b \rightarrow a+l^+l^-+b)/(dM^2 dQ^2 dy d\hat{t})$ is discussed in Eqs. (5) and (16).

For the case of coh.res, the variables \hat{t} and $z_{a'}$ can be transformed into

$$d\hat{t}_\gamma dz_{a'} = \left| \frac{D(z_{a'}, \hat{t}_\gamma)}{D(p_T, y_r)} \right| dy_r dp_T^2, \quad (27)$$

where the Jacobian determinant is

$$\begin{aligned}
& \left| \frac{D(z_{a'}, \hat{t}_\gamma)}{D(p_T, y_r)} \right| = \frac{\cosh y_r}{y x_b s_{NN} \sqrt{\cosh^2 y_r M_T^2 - M^2}} \left[e^{-2y_r} M_T \left(2 \cosh y_r \right. \right. \\
& \quad \left. \left. + \frac{2 \cosh^2 y_r M_T^2 - M^2}{M_T \sqrt{\cosh^2 y_r M_T^2 - M^2}} \right) \left(M_T \sqrt{\hat{s}_\gamma - M^2} e^{y_r} \right) \right. \\
& \quad \left. + \hat{s}_\gamma e^{-y_r} \sinh y_r \left(\frac{2 \cosh^2 y_r M_T^2 - M^2}{\cosh y_r \sqrt{\cosh^2 y_r M_T^2 - M^2}} + 2M_T \right) \right], \quad (28)
\end{aligned}$$

the invariant cross section of large p_T dileptons with p_T distribution is given by

$$\begin{aligned}
& \frac{d\sigma_{yrc}^{\text{coh.res.}}(p+p \rightarrow p+l^+l^-+X)}{dM^2 dp_T^2 dy_r} \\
&= 2 \sum_b \sum_{a'} \int dQ^2 dy dx_b f_{b/p}(x_b, \mu_b^2) f_\gamma(z_{a'}, \mu_\gamma^2) \\
& \quad \times \frac{\hat{s}_\gamma^{\frac{3}{2}}}{y x_b s_{NN} p_T} \frac{\alpha y \rho_{\text{coh}}^{++}}{2\pi Q^2} \frac{d\sigma(a'+b \rightarrow l^+l^-+b)}{dM^2 d\hat{t}}. \quad (29)
\end{aligned}$$

The invariant cross section of large p_T dileptons produced by incoh.res with p_T distribution can be written as

$$\begin{aligned}
& \frac{d\sigma_{yrc}^{\text{incoh.res.}}(p+p \rightarrow X_A + l^+l^- + X)}{dM^2 dp_T^2 dy_r} \\
&= 2 \sum_{a,b} \sum_{a'} \int dQ^2 dy dx_a dx_b f_{a/p}(x_a, \mu_a^2) f_{b/p}(x_b, \mu_b^2) \\
& \quad \times f_\gamma(z_{a'}, \mu_\gamma^2) \frac{\hat{s}_\gamma^{\frac{3}{2}}}{y x_a x_b s_{NN} p_T} e_a^2 \frac{\alpha y \rho_{\text{incoh}}^{++}}{2\pi Q^2} \\
& \quad \times \frac{d\sigma(a'+b \rightarrow l^+l^-+b)}{dM^2 d\hat{t}}, \quad (30)
\end{aligned}$$

where the cross sections of subprocesses $a'+b \rightarrow l^+l^-+b$ are discussed in Eq. (19), and the Mandelstam variables for res.pho are the same as Eq. (22) but for $Q^2 = 0$.

C. The Q^2 distribution of large p_T real photon production

The invariant cross sections of large p_T real photons can be derived from the invariant cross sections of large p_T dileptons produced by photoproduction processes if the invariant mass of dileptons is zero ($M^2 = 0$). The invariant cross section of large p_T real photons produced by coh.dir with Q^2 distribution satisfy the following form

$$\begin{aligned}
& \frac{d\sigma^{\text{coh.dir}}(p+p \rightarrow p+\gamma+X)}{dQ^2} \\
&= 2 \sum_b \int dy dx_b d\hat{t} f_{b/p}(x_b, \mu_b^2) \frac{d\sigma(p+b \rightarrow p+\gamma+b)}{dQ^2 dy d\hat{t}}, \quad (31)
\end{aligned}$$

where the cross section of subprocess $p+b \rightarrow p+\gamma+b$ is similar to Eq. (11), but the transverse and longitudinal cross sections of subprocesses $\gamma^*+b \rightarrow \gamma+b$ should be presented as the following forms

$$\begin{aligned}
& \frac{d\hat{\sigma}_T}{d\hat{t}}(\gamma^*+b \rightarrow \gamma+b) = \frac{4\pi\alpha^2 e_b^4 z^2}{Q^4} \left[-\frac{\hat{t}}{\hat{s}} - \frac{\hat{s}}{\hat{t}} + 2Q^2 \frac{\hat{u}}{\hat{s}\hat{t}} \right] \\
& \quad + \frac{8\pi\alpha^2 e_b^4 z^2}{Q^2} \frac{\hat{u}}{(\hat{s}+Q^2)^2}, \quad (32)
\end{aligned}$$

and

$$\frac{d\hat{\sigma}_L}{d\hat{t}}(\gamma^*+b \rightarrow \gamma+b) = \frac{8\pi\alpha^2 e_b^4 z^2}{Q^2} \frac{\hat{u}}{(\hat{s}+Q^2)^2}, \quad (33)$$

where the Mandelstam variables are $\hat{s} = M^2/z_q + p_T^2/(z_q - z_q^2)$, $\hat{t} = (z_q - 1)y x_b s_{NN}$, and $\hat{u} = -z_q y x_b s_{NN}$.

The invariant cross section of large p_T real photons produced by incoh.dir with Q^2 distribution can be expressed as

$$\begin{aligned} & \frac{d\sigma^{\text{incoh.dir}}(p + p \rightarrow X_A + \gamma + X)}{dQ^2} \\ &= 2 \sum_{a,b} \int dy dx_a dx_b d\hat{t} f_{a/p}(x_a, \mu_a^2) f_{b/p}(x_b, \mu_b^2) \\ & \quad \times \frac{d\sigma(a + b \rightarrow a + \gamma + b)}{dQ^2 dy d\hat{t}}, \end{aligned} \quad (34)$$

here we have $\hat{s} = M^2/z_q + p_T^2/(z_q - z_q^2)$, $\hat{t} = (z_q - 1) y x_a x_b s_{NN}$, and $\hat{u} = -z_q y x_a x_b s_{NN}$. The partonic cross sections of $a + b \rightarrow a + \gamma + b$ are analogous with Eq. (16).

In the case of coh.res, the invariant cross section for large p_T real photons with Q^2 distribution has the form

$$\begin{aligned} & \frac{d\sigma^{\text{coh.res.}}(p + p \rightarrow p + \gamma + X)}{dQ^2} \\ &= 2 \sum_b \sum_{a'} \int dy dx_b dz_a d\hat{t} f_{b/p}(x_b, \mu_b^2) f_\gamma(z_a, \mu_\gamma^2) \\ & \quad \times \frac{\alpha y \rho_{\text{coh}}^{++} d\sigma(a' + b \rightarrow \gamma + b)}{2\pi Q^2 d\hat{t}}, \end{aligned} \quad (35)$$

the cross sections of subprocesses $a' + b \rightarrow \gamma + b$ are given by [26]

$$\begin{aligned} \frac{d\hat{\sigma}}{d\hat{t}}(q\bar{q} \rightarrow \gamma\gamma) &= \frac{2\pi\alpha^2 e_q^4}{3 \hat{s}_\gamma^2} \left(\frac{\hat{t}_\gamma}{\hat{u}_\gamma} + \frac{\hat{u}_\gamma}{\hat{t}_\gamma} \right), \\ \frac{d\hat{\sigma}}{d\hat{t}}(q\bar{q} \rightarrow \gamma g) &= \frac{8\pi\alpha\alpha_s e_q^2}{9 \hat{s}_\gamma^2} \left(\frac{\hat{t}_\gamma}{\hat{u}_\gamma} + \frac{\hat{u}_\gamma}{\hat{t}_\gamma} \right), \\ \frac{d\hat{\sigma}}{d\hat{t}}(qg \rightarrow \gamma q) &= \frac{1\pi\alpha\alpha_s e_q^2}{3 \hat{s}_\gamma^2} \left(-\frac{\hat{t}_\gamma}{\hat{s}_\gamma} - \frac{\hat{s}_\gamma}{\hat{t}_\gamma} \right), \end{aligned} \quad (36)$$

where the Mandelstam variables for the subprocesses of res.pho can be written as $\hat{s}_\gamma = M^2/z'_q + p_T^2/(z'_q - z_q^2)$, $\hat{t}_\gamma = (z'_q - 1)\hat{s}_\gamma$, and $\hat{u}_\gamma = -z'_q \hat{s}_\gamma$.

For the case of incoh.res, the invariant cross section of large p_T real photons with Q^2 distribution can be written as

$$\begin{aligned} & \frac{d\sigma^{\text{incoh.res.}}(p + p \rightarrow X_A + \gamma + X)}{dQ^2} \\ &= 2 \sum_{a,b} \sum_{a'} \int dy dx_a dx_b dz_a d\hat{t} f_{a/p}(x_a, \mu_a^2) f_{b/p}(x_b, \mu_b^2) \\ & \quad \times f_\gamma(z_a, \mu_\gamma^2) e_a^2 \frac{\alpha y \rho_{\text{incoh}}^{++} d\sigma(a' + b \rightarrow \gamma + b)}{2\pi Q^2 d\hat{t}}, \end{aligned} \quad (37)$$

where the cross sections of subprocesses $a' + b \rightarrow \gamma + b$ are the same as Eq. (36).

D. The p_T distribution of large p_T real photon production

The invariant cross section of large p_T real photons produced by coh.dir with p_T distribution reads:

$$\begin{aligned} & E \frac{d\sigma_{\text{yre}}^{\text{coh.dir}}(p + p \rightarrow p + \gamma + X)}{d^3 p} \\ &= \frac{2}{\pi} \sum_b \int dQ^2 dy f_{b/p}(x_b, \mu_b^2) \frac{\hat{s}}{y s_{NN} p_T} \left(\sqrt{\hat{s}} + \frac{Q^2}{\sqrt{\hat{s}}} \right) \\ & \quad \times \frac{d\sigma(p + b \rightarrow p + \gamma + b)}{dQ^2 dy d\hat{t}}, \end{aligned} \quad (38)$$

the cross sections $d\sigma(p + b \rightarrow p + \gamma + b)/(dQ^2 dy d\hat{t})$ are discussed in Eq. (11). And for the case of incoh.dir, the invariant cross section of large p_T real photons with p_T distribution is

$$\begin{aligned} & E \frac{d\sigma_{\text{yre}}^{\text{incoh.dir}}(p + p \rightarrow X_A + \gamma + X)}{d^3 p} \\ &= \frac{2}{\pi} \sum_{a,b} \int dQ^2 dy dx_a f_{a/p}(x_a, \mu_a^2) f_{b/p}(x_b, \mu_b^2) \\ & \quad \times \frac{\hat{s}}{y x_a s_{NN} p_T} \left(\sqrt{\hat{s}} + \frac{Q^2}{\sqrt{\hat{s}}} \right) \frac{d\sigma(a + b \rightarrow a + \gamma + b)}{dQ^2 dy d\hat{t}}, \end{aligned} \quad (39)$$

the cross sections $d\sigma(a + b \rightarrow a + \gamma + b)/(dQ^2 dy d\hat{t})$ are discussed in Eq. (16). The Mandelstam variables for dir.pho are the same as Eq. (22) but for $M^2 = 0$.

The invariant cross section of large p_T real photons produced by coh.res with p_T distribution can be written as:

$$\begin{aligned} & E \frac{d\sigma_{\text{yre}}^{\text{coh.res.}}(p + p \rightarrow p + \gamma + X)}{d^3 p} \\ &= \frac{2}{\pi} \sum_b \sum_{a'} \int dQ^2 dy dx_b f_{b/p}(x_b, \mu_b^2) f_\gamma(z_a, \mu_\gamma^2) \\ & \quad \times \frac{\hat{s}_\gamma^{\frac{3}{2}}}{y x_b s_{NN} p_T} \frac{\alpha y \rho_{\text{coh}}^{++} d\sigma(a' + b \rightarrow \gamma + b)}{2\pi Q^2 d\hat{t}}, \end{aligned} \quad (40)$$

the invariant cross section of large p_T real photons produced by incoh.res with p_T distribution is given by:

$$\begin{aligned} & E \frac{d\sigma_{\text{yre}}^{\text{incoh.res.}}(p + p \rightarrow X_A + \gamma + X)}{d^3 p} \\ &= \frac{2}{\pi} \sum_{a,b} \sum_{a'} \int dQ^2 dy dx_a dx_b f_{a/p}(x_a, \mu_a^2) f_{b/p}(x_b, \mu_b^2) \\ & \quad \times f_\gamma(z_a, \mu_\gamma^2) \frac{\hat{s}_\gamma^{\frac{3}{2}}}{y x_a x_b s_{NN} p_T} e_a^2 \frac{\alpha y \rho_{\text{incoh}}^{++}}{2\pi Q^2} \\ & \quad \times \frac{d\sigma(a' + b \rightarrow \gamma + b)}{d\hat{t}}, \end{aligned} \quad (41)$$

the cross sections of subprocesses $a' + b \rightarrow \gamma + b$ are the same as Eq. (36), and the Mandelstam variables for res.pho are the same as Eq. (22), but for $Q^2 = 0$ and $M^2 = 0$.

E. The equivalent photons approximation

The idea of EPA approach is treating the field of a fast charged particle as a flux of photons. An essential advantage of EPA is that, when using it, it is sufficient to know the photo-absorption cross section on the mass shell only. Details of its off mass shell behavior are not essential. Thus, the EPA approach, as a useful technique, has been widely used to obtain the various cross sections for charged particles in relativistic heavy ion collisions [17]. Unfortunately, the accuracy of EPA and its applicability range are often neglected [10–13]. The choice of $Q_{\max}^2 \sim \hat{s}$ or ∞ is used instead of the significant dynamical cut off Λ_γ^2 which represents the precision of the EPA approach. However, the exact treatment developed above can be returned to EPA approach by taking $Q^2 \rightarrow 0$, and the detailed discussion can be found in Ref. [17]. This provides us the powerful comparisons between our results and the ones in the literatures [11,12]. Taking $Q^2 \rightarrow 0$ is corresponding to that the photon is emitted parallelly from proton or quark, and the variable y becomes the usual momentum fraction ($y = q^+/P_A^+$ for coh.pho and $y = q^+/p_a^+$ for incoh.pho) in the light-front formalism. Since the collinear factorization framework is used for the parton distribution functions, x_a and x_b are also equal to p_a^+/P_A^+ and p_b^+/P_B^+ , respectively.

The cross section of subprocess $p + b \rightarrow p + l^+l^- + b$ with EPA form reads:

$$\begin{aligned} \frac{d\sigma^{\text{coh.pho}}}{dydQ^2d\hat{t}} &= \left(\frac{\alpha y \rho_{\text{coh}}^{++}}{2\pi Q^2} \right) \frac{d\sigma}{d\hat{t}} \\ &= \frac{\alpha F_1^2(Q^2)}{2\pi Q^2} \left[\frac{1 + (1-y)^2}{y} - y \frac{2m_p^2}{Q^2} \right] \frac{d\sigma}{d\hat{t}} \\ &= \frac{df_\gamma|_{\text{coh}}(y) d\sigma}{dQ^2 d\hat{t}}, \end{aligned} \quad (42)$$

where $f_\gamma|_{\text{coh}}(y)$ is the coherent photon flux which is associated with the whole proton [28]. It should be noted that, since σ_T and σ_L are multiplied by the factor Q^{-2} , σ_L and the terms which are proportional to Q^2 in σ_T can also provide the nonzero contributions when $Q^2 \rightarrow 0$, but they are neglected in EPA approach. Actually, the errors from these omissions are so small, and can not cause any noticeable effects.

Another approximate analytic form of the coherent photon flux is developed by Drees and Zeppenfeld (DZ) [19], which is widely used in the literatures [12–14,35]. By setting $Q_{\max}^2 \rightarrow \infty$, and neglecting the m_p^2 term in ρ_{coh}^{++} , they obtained

$$f_\gamma|_{\text{coh}}(y) = \frac{\alpha}{2\pi} \frac{1 + (1-y)^2}{y} \left[\ln A - \frac{11}{6} + \frac{3}{A} - \frac{3}{2A^2} + \frac{1}{3A^2} \right], \quad (43)$$

where $A = (1 + 0.71 \text{ GeV}^2/Q_{\min}^2)$.

For the case of incoh.pho, the cross section of subprocess $a + b \rightarrow a + l^+l^- + b$ with EPA form reads:

$$\begin{aligned} \frac{d\sigma^{\text{incoh.pho}}}{dydQ^2d\hat{t}} &= \left(e_a^2 \frac{\alpha y \rho_{\text{incoh}}^{++}}{2\pi Q^2} \right) \frac{d\sigma}{d\hat{t}} \\ &= e_a^2 \frac{\alpha}{2\pi} \frac{1 - F_1^2(Q^2)}{Q^2} \frac{1 + (1-y)^2}{y} \frac{d\sigma}{d\hat{t}} \\ &= \frac{df_\gamma|_{\text{incoh}}(y) d\sigma}{dQ^2 d\hat{t}}, \end{aligned} \quad (44)$$

where $f_\gamma|_{\text{incoh}}(y)$ is the incoherent photon flux.

Another form of Eq. (44), which neglects the $F_1^2(Q^2)$ term and takes $Q_{\min}^2 = 1 \text{ GeV}^2$, is

$$f_\gamma|_{\text{incoh}}(y) = e_a^2 \frac{\alpha}{2\pi} \frac{1 + (1-y)^2}{y} \ln \frac{Q_{\max}^2}{Q_{\min}^2}. \quad (45)$$

III. NUMERICAL RESULTS

The several theoretical inputs and the bounds of involved variables need to be provided. The mass range of dileptons is chosen as $200 \text{ MeV} < M < 750 \text{ MeV}$, the mass of proton is $m_p = 0.938 \text{ GeV}$ [36]. Since the large p_T photo-production processes are considered (the contribution are mainly from the transverse direction), the rapidity is set to be $y_r = 0$ ($\theta_c \sim \pi/2$) according to Ref. [11].

For the Q^2 distribution, the bounds of integration variables for coh.dir are given by

$$\begin{aligned} \hat{t}_{\min} &= (z_{q\min} - 1)yx_b s_{NN}, \\ \hat{t}_{\max} &= (z_{q\max} - 1)yx_b s_{NN}, \\ x_{b\min} &= \frac{\hat{s}_{\min} + Q^2}{y s_{NN}}, \quad x_{b\max} = 1, \\ y_{\min} &= \frac{\hat{s}_{\min} + Q^2}{s_{NN}}, \\ y_{\max} &= \frac{1}{2m_p^2} \sqrt{4m_p^2 Q^2 + Q^4} + \frac{2m_p^2 - s_{NN}}{2m_p^2 s_{NN}} Q^2, \end{aligned} \quad (46)$$

where $\hat{s}_{\min} = (M_{T\min} + p_{T\min})^2$, $p_T^2 = \hat{t}(\hat{s} \hat{u} + Q^2 M^2)/(\hat{s} + Q^2)^2$ is the square of the transverse momentum for dileptons and

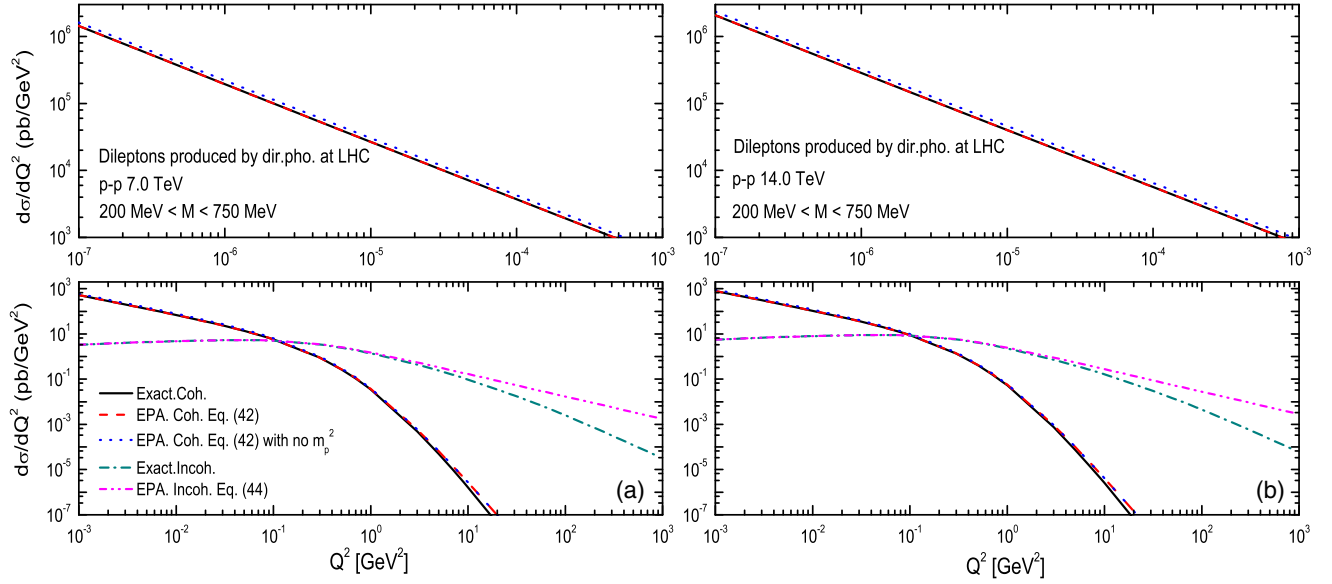


FIG. 5. (a) Comparisons of the exact results and EPA ones of dileptons produced by dir.pho for $y_r = 0$. The solid line (black) represents the exact results of coh.pho, the dash line (red) represents the results of EPA based on the photon flux function Eq. (42), the dot line (blue) represents the results of EPA based on Eq. (42) but without m_p^2 term, the dash-dot line (dark-cyan) represents the exact results of incoh.pho, the dash-dot-dot line (magenta) represents the results of EPA based on the photon flux function of Eq. (44). (b) The same as figure (a) but for p-p collisions at $\sqrt{s_{NN}} = 14.0$ TeV. The solid line (black) coincides with the dash line (red) in small Q^2 domain. Since the contributions of incoh.pho are so small comparing with coh.pho in the small Q^2 domain, its results are not plotted in the upper figures.

$$z_{q \min} = \frac{M^2 + \hat{s}}{2\hat{s}} - \frac{\sqrt{(\hat{s} - M^2)^2 - 4p_{T \min}^2 \hat{s}}}{2\hat{s}}$$

$$z_{q \max} = \frac{M^2 + \hat{s}}{2\hat{s}} + \frac{\sqrt{(\hat{s} - M^2)^2 - 4p_{T \min}^2 \hat{s}}}{2\hat{s}}. \quad (47)$$

The bounds of variables for the incoh.dir are same as Eq. (46), but for $\hat{t}_{\min} = (z_{q \min} - 1)yx_a x_b s_{NN}$, $\hat{t}_{\max} = (z_{q \max} - 1)yx_a x_b s_{NN}$, $x_{b \min} = (\hat{s}_{\min} + Q^2)/yx_a s_{NN}$, $x_{a \min} = (\hat{s}_{\min} + Q^2)/ys_{NN}$ and $x_{a \max} = 1$.

In the coh.res, the bounds of variables are

$$\hat{t}_{\gamma \min} = (z'_{q \min} - 1)z_a y x_b s_{NN},$$

$$\hat{t}_{\gamma \max} = (z'_{q \max} - 1)z_a y x_b s_{NN},$$

$$z_{a \min} = \frac{\hat{s}_{\gamma \min}}{y x_b s_{NN}},$$

$$z_{a \max} = 1,$$

$$x_{b \min} = \frac{\hat{s}_{\gamma \min}}{z_{a \max} y s_{NN}},$$

$$x_{b \max} = 1,$$

$$y_{\min} = \frac{\hat{s}_{\gamma \min}}{z_{a \max} s_{NN}}, \quad (48)$$

y_{\max} is same as Eq. (46), where $\hat{s}_{\gamma \min} = (M_{T \min} + p_{T \min})^2$, $p_T^2 = \hat{t} \hat{u} / \hat{s}$ and

$$z'_{q \min} = \frac{M^2 + \hat{s}_{\gamma}}{2\hat{s}_{\gamma}} - \frac{\sqrt{(\hat{s}_{\gamma} - M^2)^2 - 4p_{T \min}^2 \hat{s}_{\gamma}}}{2\hat{s}_{\gamma}}$$

$$z'_{q \max} = \frac{M^2 + \hat{s}_{\gamma}}{2\hat{s}_{\gamma}} + \frac{\sqrt{(\hat{s}_{\gamma} - M^2)^2 - 4p_{T \min}^2 \hat{s}_{\gamma}}}{2\hat{s}_{\gamma}}. \quad (49)$$

The bounds of variables for the incoh.res are same as Eq. (48) but for $\hat{t}_{\gamma \min} = (z'_{q \min} - 1)z_a y x_a x_b s_{NN}$, $\hat{t}_{\gamma \max} = (z'_{q \max} - 1)z_a y x_a x_b s_{NN}$, $z_{a \min} = \hat{s}_{\gamma \min} / (y x_a x_b s_{NN})$, $x_{b \min} = \hat{s}_{\gamma \min} / (z_{a \max} y x_a s_{NN})$, $x_{a \min} = \hat{s}_{\gamma \min} / (z_{a \max} y s_{NN})$ and $x_{a \max} = 1$.

For the p_T distribution, the bounds of x_a , x_b and y are same as Q^2 distribution, but for $z_{a \max} = 1 / (1 + Q^2 / (4p_T^2))$ [37,38], the bounds of Q^2 are $Q_{\min}^2 |_{\text{coh.dir}} = x_1^2 m_p^2 / (1 - x_1)$, $x_1 = \hat{s} / s_{NN}$, $Q_{\min}^2 |_{\text{incoh.dir}} = 0$, $Q_{\min}^2 |_{\text{coh.res}} = Q_{\min}^2 |_{\text{incoh.res}} = 0.01 \text{ GeV}^2$ [39], and $Q_{\max}^2 = 4p_T^2$ is used for the exact calculations and the EPA ones Eqs. (42) and (44).

In Figs. 5 and 6, the Q^2 distribution of dileptons produced by photoproduction processes in p-p collisions at LHC energies are plotted. The contribution of exact treatment are compared with the EPA ones. For the case of coh.dir, the results of EPA share the same trend with the exact one in the small Q^2 region, since EPA is obtained by setting the photon virtuality $Q^2 \rightarrow 0$ and neglecting the longitudinal photon contributions. Considering that the coherent photon flux function with the DZ form Eq. (43)

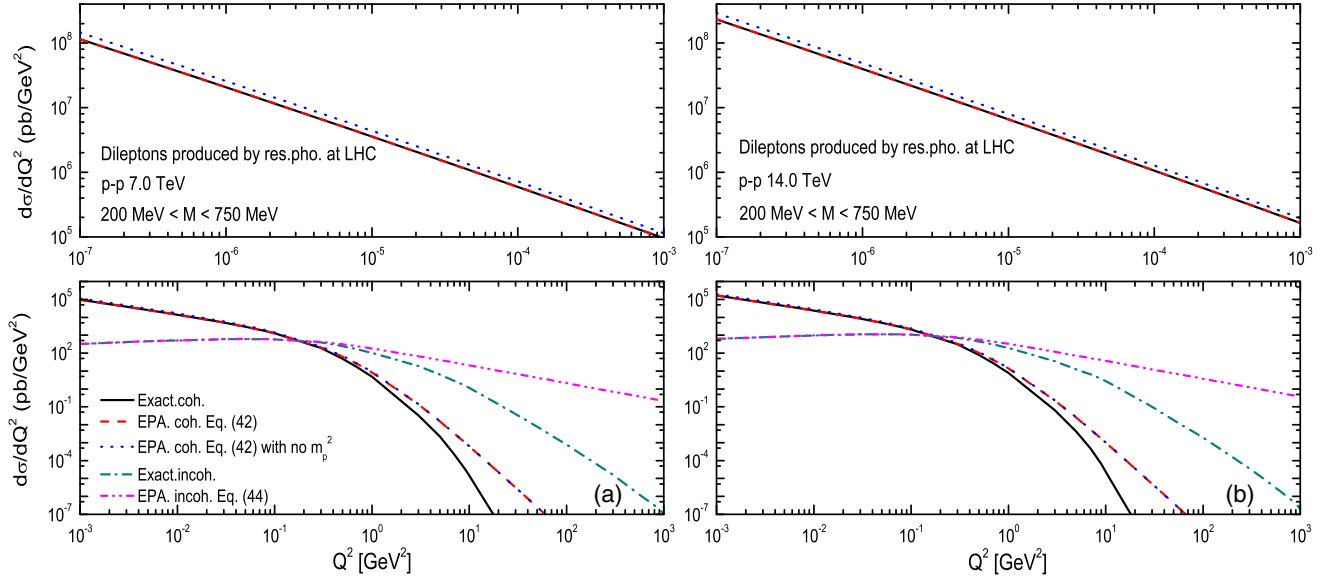


FIG. 6. Same as Fig. 5 but for res.pho.

is obtained by neglecting the m_p^2 term, the EPA result Eq. (42) with no m_p^2 term is also presented for researching the Q^2 dependence behavior and the validity of Eq. (43). It can be seen that, the EPA result with no m_p^2 term is greater than the result of Eq. (42) at small Q^2 domain, but they become consistent with increasing Q^2 , since the m_p^2 term is inversely proportional to Q^2 . The exact result is in agreement with the EPA results Eq. (42) in small Q^2 region, and is less than the EPA ones when $Q^2 > 10 \text{ GeV}^2$. The case of coh.res is similar to coh.dir, but the differences between the exact results and the EPA ones are much more evident in large Q^2 domain. Therefore, the EPA approach is only suitable in the small Q^2 domain, and can be used as a good approximation for coh.pho, since the small Q^2 domain give the main contribution which agree with the statements of Martin and Ryskin in Ref. [29], and of Budnev and Ginzburg in Ref. [17]. And the errors from the omission of m_p^2 term in Eq. (42) and the option of $Q_{\text{max}}^2 \sim \hat{s}$ or ∞ in Eqs. (42) and (43) cannot be neglected.

For the case of incoh.dir, the exact result and the EPA ones are almost same and can be neglected comparing with coh.dir when $Q^2 < 0.01 \text{ GeV}^2$, but the differences among them are evident when $Q^2 > 0.1 \text{ GeV}^2$. Besides, the incoh.dir contribution is comparable with the coh.dir contribution when $Q^2 > 0.01 \text{ GeV}^2$, and becomes much larger when $Q^2 > 0.1 \text{ GeV}^2$. The case of incoh.res is similar to incoh.dir, but the differences between the exact results and the EPA ones are more prominent in large Q^2 domain. It should be emphasized that, if the Martin-Ryskin method is not considered, the incoh.pho contribution will always much larger than the coh.pho one in the whole Q^2 region and is divergent at very small Q^2 domain ($Q^2 \rightarrow 0$). This is an unphysical result. Comparing with the Martin-Ryskin

method which avoid this unphysical large value of incoh.pho naturally, the physical interpretation is not clear in literatures [9,11–14] which calculated the incoh.pho contribution by using the artificial cutoff $Q^2 > 1 \text{ GeV}^2$. Therefore, the EPA approach is not a effective approximation for incoh.pho, since the incoh.pho contribution are mainly from the large Q^2 domain where the errors are obvious, and the results in these works are not accurate enough.

The p_T distribution of dileptons produced by photoproduction processes in p-p collisions at LHC energies are illustrated in Figs. 7 and 8. For the case of coh.dir, the exact result nicely agrees with EPA one Eq. (42) in the whole p_T region. However, the result of Eq. (43) is much larger than the results of exact treatment and Eq. (42), since Eq. (43) is obtained by neglecting the m_p^2 term in Eq. (42), and setting $Q_{\text{max}}^2 = \infty$ which will cause obvious errors. It can be seen that, the contribution of res.pho is about two orders of magnitude larger than the dir.pho, thus the contribution of large p_T dileptons produced by photoproduction processes is mainly from res.pho. The case of coh.res is similar to coh.dir, the errors from Eq. (43) is also prominent. Therefore, the choice of Q_{max}^2 is crucial to the accuracy of EPA. Equation (42) with $Q_{\text{max}}^2 = 4p_T^2$ is a good choice for calculating coh.pho. However, choosing $Q^2 \sim \infty$ will cause the large fictitious contribution from the large Q^2 domain (it can be found in the figures which show the Q^2 dependence behavior), which agree with the statements in Ref. [17]. For the practical use of EPA, except considering the kinematically allowed Q^2 -change region, one should also elucidate whether there is a dynamical cut off Λ_γ^2 , and estimate it. However, the definite values of the Λ_γ^2 for different processes are essentially different, and still need further studies.

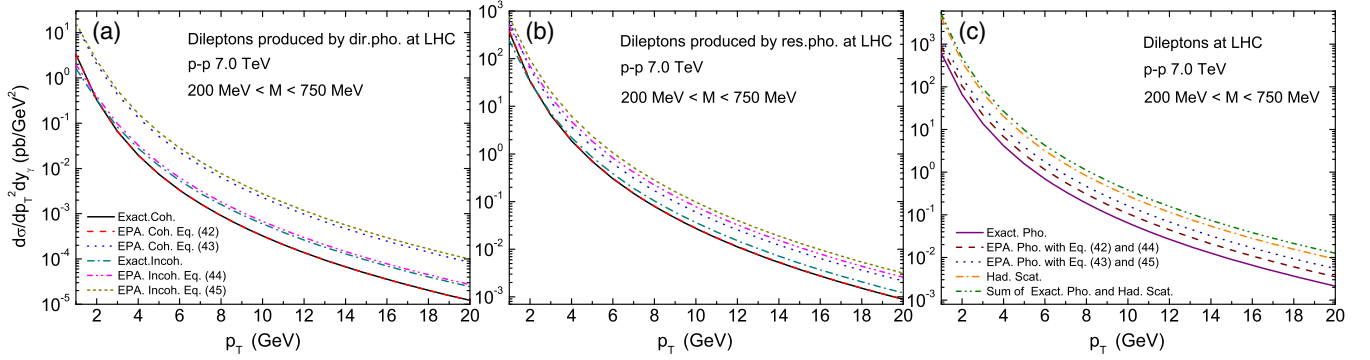


FIG. 7. (a) Invariant cross section of dileptons produced by dir.pho. for $y_r = 0$ in p-p collisions at $\sqrt{s_{NN}} = 7.0$ TeV. (b) Same as (a) but for res.pho. (c) The comparisons between the photoproduction processes results with the ones of hadronic processes, the solid line (purple) represents the exact results of photoproduction processes, the dash line (wine) represents the results of EPA based on Eqs. (42) and (44), the dot line (royal) represents the results of EPA based on Eqs. (43) and (45), the dash-dot line (orange) represents the results of hard scattering of initial partons (had.scatt), the dash-dot-dot line (olive) represents the sum of the exact results of photoproduction processes and the ones of had.scatt. In Figs. 7(a) and 7(b), the solid line (black) coincides with the dash line (red) in the whole p_T domain.

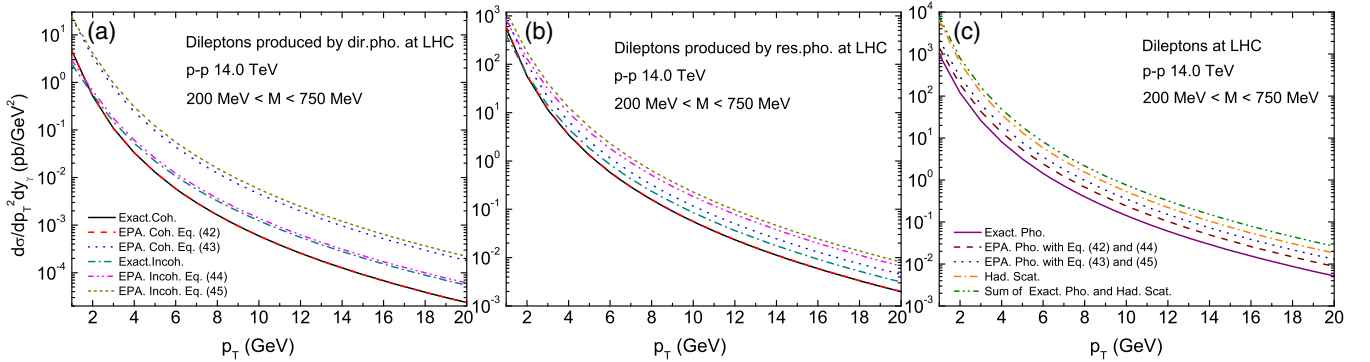


FIG. 8. Same as Fig. 7 but for p-p collisions at $\sqrt{s_{NN}} = 14$ TeV.

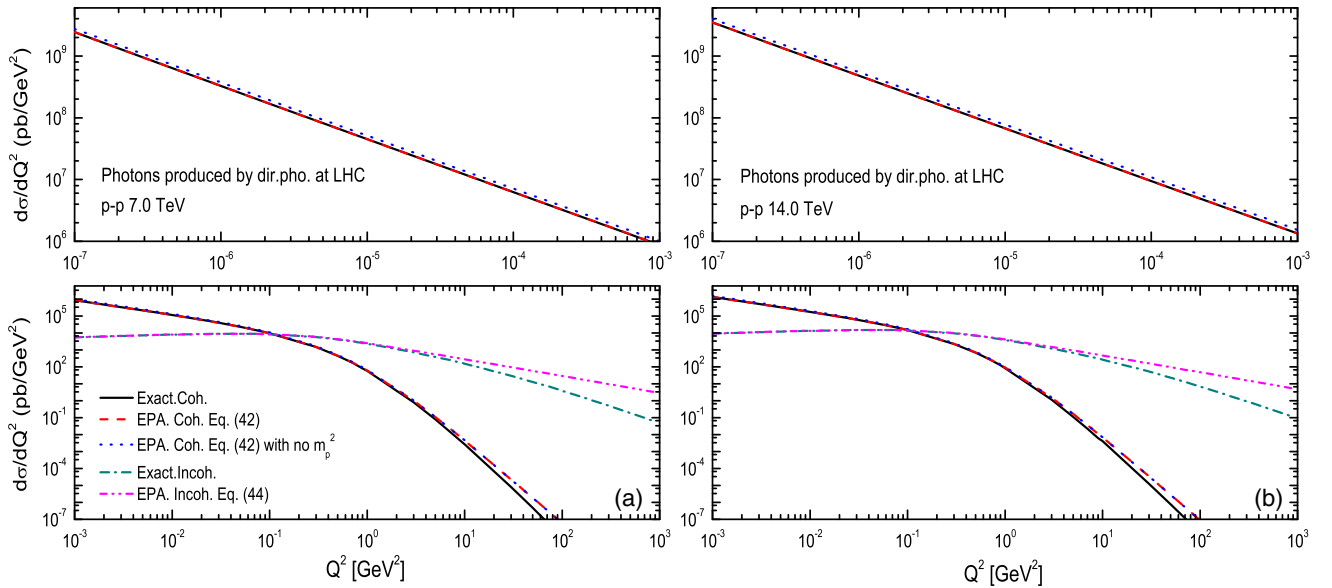


FIG. 9. Photons produced by dir.pho. for $y_r = 0$ in p-p collisions at $\sqrt{s_{NN}} = 7.0$ TeV (a) and at $\sqrt{s_{NN}} = 14.0$ TeV (b). The solid line (black) coincides with the dash line (red) in small Q^2 domain. Since the contributions of incoh.pho are so small comparing with coh.pho in the small Q^2 domain, its results are not plotted in the upper figures.

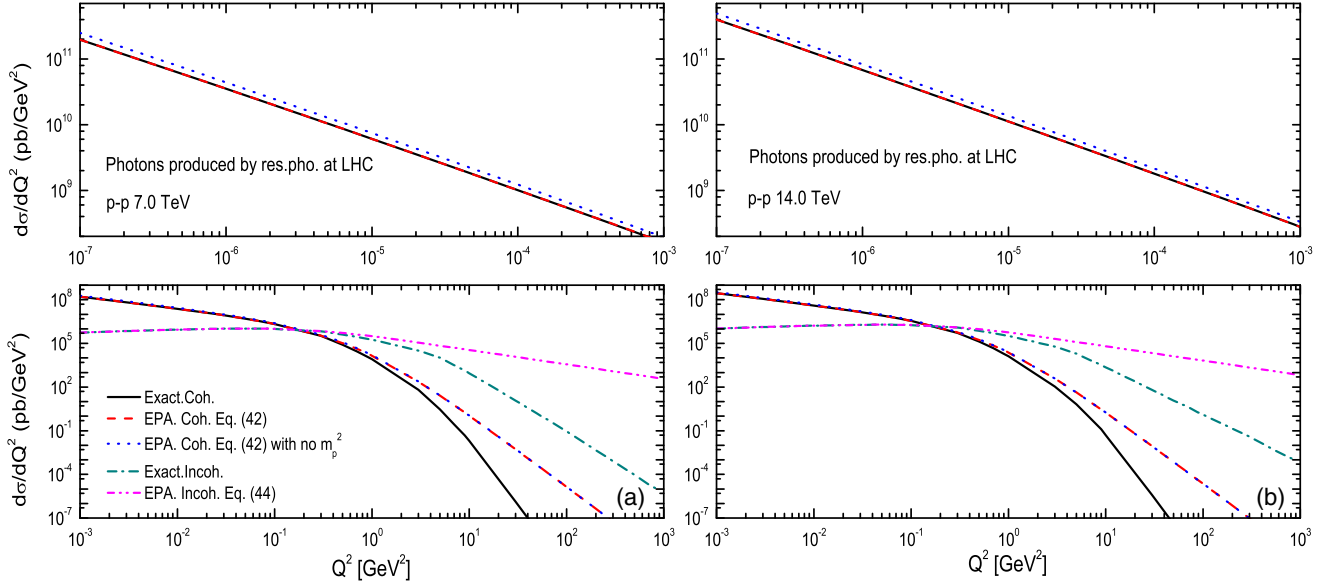


FIG. 10. Same as Fig. 9 but for res.pho.

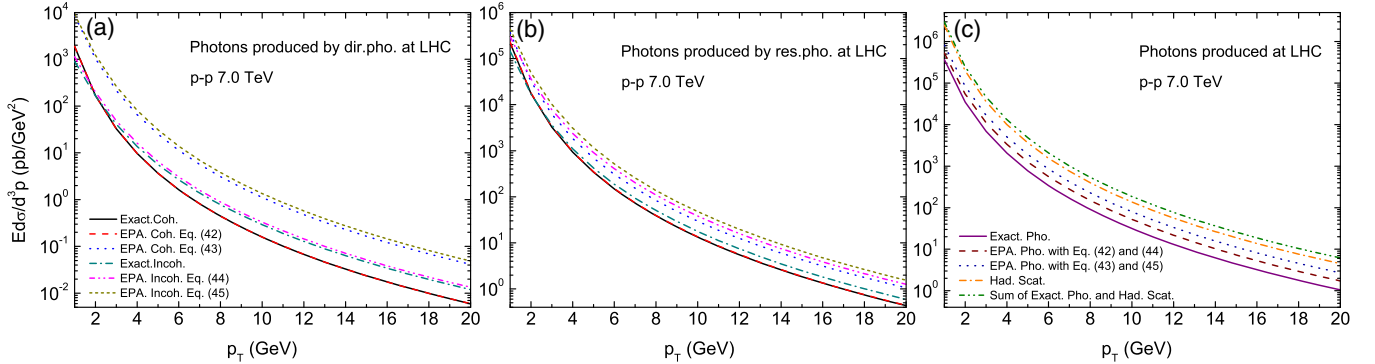


FIG. 11. (a) Invariant cross section of photons produced by dir.pho for $y_r = 0$ in p-p collisions at $\sqrt{s_{NN}} = 7.0$ TeV. (b) Same as (a) but for res.pho. (c) The comparisons between the photoproduction processes results with the ones of hadronic processes. In Figs. 11(a) and 11(b), the solid line (black) coincides with the dash line (red) in the whole p_T domain.

For the case of incoh.dir, the EPA results are greater than the exact one in the whole p_T region, but the difference between the EPA result Eq. (45) and the exact one is much more evident, since the Q_{\max}^2 is set by $\hat{s}/4$ in Eq. (45), which include the errors from the large Q^2 domain. The incoh.res is similar to incoh.dir, the differences between the exact result and the EPA ones are prominent in the whole p_T region. Thus, the EPA approach cannot be used in incoh.pho and the effects of the inapplicability of EPA for incoh.pho are significant. In Figs. 7(c) and 8(c), the comparisons between the photoproduction processes and the one of initial partons hard scattering are presented. It can be seen that the corrections from the exact results of photoproduction processes to had.scatt are non-negligible, especially in the large p_T domain. However, the differences between the EPA results and the exact one are evident. The EPA results will give the large fictitious correction to the

production of dileptons and photons, especially for the EPA result of Eqs. (43) and (45). Thus the statements are not accurate in Ref. [11,12], in which the incoh.pho of dileptons and photons was calculated by using the EPA approach Eq. (45) with $Q_{\max}^2 = \hat{s}/4$ and $Q_{\min}^2 = 1$ GeV², and the coh.pho was calculated by using the photon flux function with the DZ form Eq. (43).

Figures 9 and 10 present the Q^2 distribution of real photons produced by photoproduction processes in p-p collision at LHC energies. It is shown that the differences among the exact result and EPA ones are more obvious in the large Q^2 region. The p_T distribution of real photons produced by photoproduction processes in p-p collision at LHC energies can be found in Figs. 11 and 12. The results are similar to the case of dileptons in Figs. 7 and 8, but the inapplicability of EPA for incoh.pho and the errors from the option of $Q_{\max}^2 \sim \infty$ and $Q_{\max}^2 = \hat{s}/4$ are more obvious.

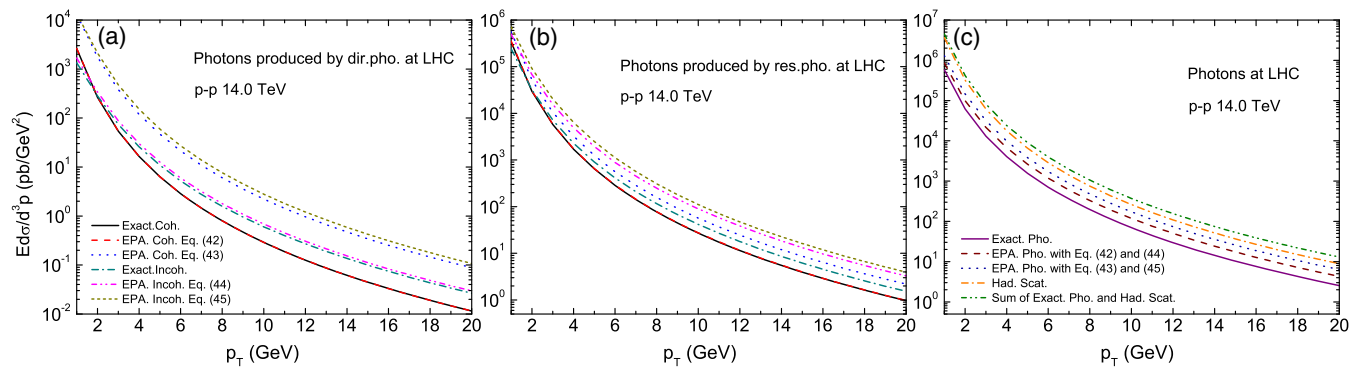


FIG. 12. Same as Fig. 11 but for p-p collisions at $\sqrt{s_{NN}} = 14$ TeV.

We also compare our results of real photons to Refs. [11,12], the inaccuracy of EPA is more evident. Therefore, the EPA can be used for coh.pho with the suitable choice of Q_{\max}^2 . And for incoh.pho, EPA is not an effective treatment, since it dominates the large Q^2 region where the errors are obvious. Thus, the exact treatment is needed to deal accurately with the photoproduction of dileptons and photons.

IV. SUMMARY AND CONCLUSIONS

We have investigated the production of large p_T dileptons and photons induced by photoproduction processes in p-p collisions at LHC energies, and presented the distributions of Q^2 and p_T . The exact treatment, which returns to the EPA approach in the limit $Q^2 \rightarrow 0$, is developed for calculations. The coherent and incoherent photon emission processes are considered simultaneously and the Martin-Ryskin method is used for avoiding the double counting. The comparisons between the exact results and EPA ones are presented for discussing the applicability range of EPA and its accuracy. The numerical results indicate that, the EPA approach is only a good approximation in the small Q^2

region and can be used for coh.pho with the suitable option of Q_{\max}^2 . For incoh.pho, EPA is not an effective approximation, since the incoh.pho dominate the large Q^2 region where the errors are obvious. The photon flux function Eq. (43) developed by Drees and Zeppenfeld and Eq. (45) with $Q_{\max}^2 = \hat{s}/4$ are widely used in the literatures [9–13,28], and the imprecise statements were given. Therefore, EPA cannot provide accurate enough results for the photoproduction of large- p_T dileptons and photons in p-p collision, and the exact treatment should be considered.

ACKNOWLEDGMENTS

We thank Yong-Ping Fu for useful communications. This work is supported in part by the National Natural Science Foundation of China (Grants No. 11747086, No. 11465021, and No. 61465015), and by the Young Backbone Teacher Training Program of Yunnan University. Z.M. is supported by Yunnan University's Research Innovation Fund for Graduate Students (Grant No. YDY17108).

-
- [1] E. Fermi, *Z. Phys.* **29**, 315 (1924).
[2] K. F. V. Weizsäcker, *Z. Phys.* **88**, 612 (1934).
[3] E. J. Williams, *Phys. Rev.* **45**, 729 (1934).
[4] L. D. Landau and E. M. Lifshitz, *Sov. Phys.* **6**, 244 (1934).
[5] G. Nordheim, L. W. Nordheim, J. R. Oppenheimer, and R. Serber, *Phys. Rev.* **51**, 1037 (1937).
[6] R. H. Dalitz and D. R. Yennie, *Phys. Rev.* **105**, 1598 (1957).
[7] I. Ya. Pomeranchuk and I. M. Shmushkevich, *Nucl. Phys.* **23**, 452 (1961).
[8] R. B. Curtis, *Phys. Rev.* **104**, 211 (1956).
[9] J. Q. Zhu, Z. L. Ma, C. Y. Shi, and Y. D. Li, *Phys. Rev. C* **92**, 054907 (2015).
[10] Y. P. Fu and Y. D. Li, *Nucl. Phys.* **A865**, 76 (2011).
[11] Y. P. Fu and Y. D. Li, *Phys. Rev. C* **84**, 044906 (2011).
[12] G. M. Yu and Y. D. Li, *Phys. Rev. C* **91**, 044908 (2015).
[13] J. Q. Zhu and Y. D. Li, *Chin. Phys. Lett.* **29**, 081301 (2012).
[14] J. Q. Zhu, Z. L. Ma, C. Y. Shi, and Y. D. Li, *Nucl. Phys.* **B900**, 431 (2015).
[15] A. J. Baltz, G. Baur, D. Denterria, L. Frankfurt, F. Gelis, V. Guzey, K. Hencken, Y. Kharlov, M. Klasen, and S. Klein, *Phys. Rep.* **458**, 1 (2008).
[16] C. J. Brown and D. H. Lyth, *Nucl. Phys.* **B53**, 323 (1973).
[17] V. M. Budnev, I. F. Ginzburg, G. V. Meledin, and V. G. Serbo, *Phys. Rep.* **15**, 181 (1975).

- [18] S. J. Brodsky, T. Kinoshita, and H. Terazawa, *Phys. Rev. D* **4**, 1532 (1971); H. Terazawa, *Rev. Mod. Phys.* **45**, 615 (1973).
- [19] M. Drees and D. Zeppenfeld, *Phys. Rev. D* **39**, 2536 (1989); B. A. Kniehl, *Phys. Lett. B* **254**, 267 (1991).
- [20] M. Drees, J. Ellis, and D. Zeppenfeld, *Phys. Lett. B* **223**, 454 (1989).
- [21] S. Frixione, M. L. Mangano, P. Nason, and G. Ridolfi, *Phys. Lett. B* **319**, 339 (1993).
- [22] R. Nisius, *Phys. Rep.* **332**, 165 (2000).
- [23] Y. D. Li and L. S. Liu, *Phys. Lett. B* **377**, 177 (1996).
- [24] M. Krawczyk, A. Zembruski, and M. Staszal, *Phys. Rep.* **345**, 265 (2001).
- [25] J. M. Butterworth, J. R. Forshaw, and M. H. Seymour, *Z. Phys. C* **72**, 637 (1996).
- [26] J. F. Owens, *Rev. Mod. Phys.* **59**, 465 (1987).
- [27] G. Baur, K. Hencken, and D. Trautmann, *J. Phys. G* **24**, 1657 (1998).
- [28] J. Q. Zhu and Y. D. Li, *Nucl. Phys.* **B904**, 386 (2016).
- [29] A. D. Martin and M. G. Ryskin, *Eur. Phys. J. C* **74**, 3040 (2014).
- [30] B. A. Kniehl and L. Zwirner, *Nucl. Phys.* **B621**, 337 (2002).
- [31] M. Glück, E. Reya, and A. Vogt, *Z. Phys. C* **53**, 127 (1992).
- [32] Z. B. Kang, J. W. Qiu, and W. Vogelsang, *Phys. Rev. D* **79**, 054007 (2009); R. D. Field, *Applications of Perturbative QCD* (Addison-Wesley Publishing Company, Reading, MA, 1989).
- [33] M. Glück, E. Reya, and I. Schienbein, *Phys. Rev. D* **60**, 054019 (1999).
- [34] Z. L. Ma, J. Q. Zhu, C. Y. Shi, and Y. D. Li, *Chin. Phys. Lett.* **32**, 121202 (2015).
- [35] N. Baron and G. Baur, *Phys. Rev. C* **49**, 1127 (1994); M. Drees, R. M. Godbole, M. Nowakowski, and S. D. Rindani, *Phys. Rev. D* **50**, 2335 (1994).
- [36] K. A. Olive *et al.* (Particle Data Group), *Chin. Phys. C* **38**, 090001 (2014).
- [37] G. Rossi, *Phys. Rev. D* **29**, 852 (1984).
- [38] M. Glück, E. Reya, and M. Stratmann, *Phys. Rev. D* **51**, 3220 (1995).
- [39] M. Glück, E. Reya, and I. Schienbein, *Eur. Phys. J. C* **10**, 313 (1999).